

The effects of Co_3O_4 on the Structure and Unusual Magnetism of LaCoO_3

A. M. Durand,¹ T. J. Hamil,¹ D. P. Belanger,¹ S. Chi,² F. Ye,²
J. A. Fernandez-Baca,³ Y. Abdollahian,⁴ and C. H. Booth⁵

¹*Department of Physics, University of California, Santa Cruz, CA 95064, USA*

²*Quantum Condensed Matter Division, Oak Ridge National Laboratory, Oak Ridge, Tennessee 37831, USA*

³*Quantum Condensed Matter Division, Oak Ridge National Laboratory,
Oak Ridge, Tennessee 37831, USA; Department of Physics and Astronomy,
University of Tennessee-Knoxville, Knoxville, TN, 37996*

⁴*Department of Chemistry, University of California, Santa Cruz, CA 95064, USA*

⁵*Chemical Sciences Division, Lawrence Berkeley National Laboratory, Berkeley, CA 94720, USA*

(Dated: March 3, 2022)

Bulk La_wCoO_3 particles with $w = 1.1, 1.0, 0.9, 0.8,$ and 0.7 were synthesized using starting materials with varying molar ratios of La_2O_3 and Co_3O_4 . The resulting particles are characterized as LaCoO_3 crystals interfaced with a crystalline Co_3O_4 phase. X-ray and neutron scattering data show little effect on the average structure and lattice parameters of the LaCoO_3 phase resulting from the Co_3O_4 content, but magnetization data indicate that the amount of Co_3O_4 strongly affects the ferromagnetic ordering at the interfaces below $T_C \approx 89$ K. In addition to ferromagnetic long-range order, LaCoO_3 exhibits antiferromagnetic behavior with an unusual temperature dependence. The magnetization for fields $20 \text{ Oe} \leq H \leq 5 \text{ kOe}$ is fit to a combination of a power law $((T - T_C)/T_C)^\beta$ behavior representing the ferromagnetic long-range order and sigmoid-convoluted Curie-Weiss-like behavior representing the antiferromagnetic behavior. The critical exponent $\beta = 0.63 \pm 0.02$ is consistent with 2D (surface) ordering. Increased Co_3O_4 correlates well to increased ferromagnetism. The weakening of the antiferromagnetism below $T \approx 40$ K is a consequence of the lattice reaching a critical rhombohedral distortion as T is decreased for core regions far from the Co_3O_4 interfaces. We introduce a model that describes the ferromagnetic behavior of the interface regions and the unusual antiferromagnetism of the core regions.

PACS numbers:

Introduction

LaCoO_3 (LCO), a rhombohedrally distorted perovskite, contains several intriguing magnetic features that have been studied for decades without being adequately explained. Many studies have been done on epitaxial strain in LCO thin films and on surface strain in LCO bulk particles. However, systematic studies examining the effects of impurity phase interface strain in the bulk particles have been lacking. In order to explore the effects of strain-induced ferromagnetism in this system further, we systematically varied the content of Co_3O_4 in LCO bulk particles, which allowed us to form a suitable model of the magnetic and structural behavior throughout the particles.

In LCO, a magnetic susceptibility maximum in large fields near $T = 40$ K has been attributed to a local thermal spin state transition associated with the Co^{3+} octahedrally-coordinated ion [1–3]. In the CoO_6 octahedra, the Co 3d and the O 2p orbitals hybridize to form lower energy t_{2g} and higher energy e_g orbitals. Within this localized spin excitation model, there has been a long-standing debate as to whether the electrons in these orbitals - presumed to be paired in a $S = 0$, low-spin (LS) configuration - excite into either a $S = 1$, intermediate-spin (IS), a $S = 2$ high-spin (HS) configuration, or a mixture of the two [4–9]. In the LS configuration ($t_{2g}^6 e_g^0$),

all of the Co^{3+} electrons are paired together in the lowest energy orbitals. In the HS configuration ($t_{2g}^4 e_g^2$), reduction of the crystal field splitting between the t_{2g} and e_g energy levels combined with the intra-atomic Hund interaction results in spins able to transition into the higher energy e_g levels. In the IS configuration ($t_{2g}^5 e_g^1$), the splitting is such that only one electron is in the e_g state; this would lead to a doubly degenerate ground state resulting in a Jahn-Teller (JT) distortion of two of the Co-O bond lengths in the CoO_6 octahedron [1].

More recently, the interpretation of the magnetism in the context of local spin state excitations has been called into question. Pair-distribution function (PDF) and Extended X-ray Absorption Fine Structure (EXAFS) studies showed no significant variation in the Co-O bond length, precluding a direct application of the Korotin model. [10, 11]. Furthermore, band structure calculations suggest that the e_g states extend over a large energy range (10 eV), which argues for the importance of the extended nature of the electron states [12, 13]. We find that the average magnetic moment of LaCoO_3 varies with temperature in a way more readily interpreted within an extended electron state picture emerging from band structure calculations [13] than one where the transitions are between spin states of localized Co ions. An extended, collective state model better describes the unusual temperature dependence of antiferromagnetic features that correlate well with structural changes near

$T = 40$ K and the weak ferromagnetic (FM) long-range order observed for $T < 89$ K.

The effects of lattice structure and strains on the ferromagnetism of LCO have been considered in previous works. In a study using dynamical mean-field theory in a local density approximation, Krapek *et al* found that a magnetic state is favored by lattice expansion and that the latter acts as positive feedback for the appearance of local moments [14]. Seo *et al* argued that strained LCO heterostructures can induce thermal spin state transitions [15]. By depositing LCO thin films onto different substrates, Fuchs *et al* successfully tuned the ferromagnetic ordering of LCO; [16] an increase in epitaxial strain between the substrate and film was observed to correlate with an increase in the effective magnetic moment μ_B/Co . A previous study suggested that ferromagnetic effects are induced by strain from Co-impurities in bulk powders of LCO [17] and that the Co-O-Co bond angle, γ , is a structural indicator of the strength of ferromagnetic ordering. Other groups, however, have singled out changes in the Co-O bond length [14, 18], the amount of rhombohedral distortion [13], or the unit cell volume [19] as direct mechanisms for ferromagnetic ordering.

Recently, a spintronic device was constructed by exploiting the strain-induced ferromagnetic long-range order in a thin film of LCO. The piezoelectric properties of a thin SrTiO₃ film allowed voltage switching of the ferromagnetism of the LCO layer [20]. Developing a fundamental understanding of the strain-dependent ferromagnetism of LCO and similar perovskite structures is a crucial step in identifying other perovskites suitable for such spintronic devices and, in particular, will guide the design of devices with ferromagnetic materials that can be switched at more practical temperatures. More comprehensive models must address the collective behaviors associated with the strain-switched ferromagnetism.

In order to examine the effects of strain on bulk LCO, we varied the amount of Co₃O₄ phase in the bulk particles by varying the starting materials used in the synthesis. The resulting powder samples are La_wCoO₃, with $w = 0.7, 0.8, 0.9, 1.0$ and 1.1 . The nonstoichiometry is not expressed uniformly across the samples. Instead, as will be discussed, in addition to large crystalline regions of LCO, well-formed crystals of Co oxide-based impurity phases form. This suggests, to a good approximation, that particles consist of regions of LaCoO₃ interfacing with crystalline impurity phases, predominately that of Co₃O₄. The structure and magnetic properties of the particles were characterized using x-ray diffraction, neutron diffraction, and magnetometry. In this report, we review the sample synthesis and discuss the sample stoichiometry. We then present structural results from x-ray and neutron diffraction. Next, we discuss results from SQUID magnetometry. Finally, we discuss a model of the structural and magnetic behaviors in terms of two types of regions, interface regions near interfaces between

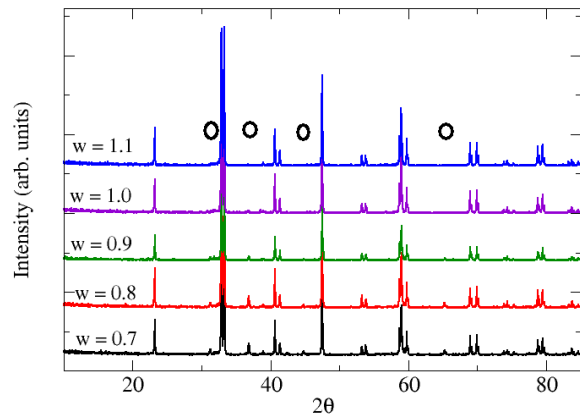


FIG. 1: X-ray diffraction spectra for all samples at room temperature. Co₃O₄ structural peak positions are marked by an oval. The spectra are vertically offset for clarity.

LCO and impurity phases and at LCO surfaces and core regions far from such interfaces.

Synthesis

The samples were synthesized using a standard solid state reaction. The bulk Co₃O₄ and La₂O₃ were ground together using a mortar and pestle and then heated to 850°C - 1050°C for approximately 8 hours in air. The grinding and heating processes were repeated five times, with a final 24 hour heating at 1100°C in most cases. X-ray powder diffraction characterizations before and after that heating showed no differences for the final 24 hour heating; it was not applied to the $w = 0.9$ sample used for x-ray diffraction analysis and magnetometry.

X-Ray and Neutron Diffraction

X-ray scattering data were taken using a Rigaku SmartLab powder diffractometer equipped with a copper x-ray tube (λ (Cu K $_{\alpha}$) = 1.54056 Å, tube energy 44 mA / 40 kV). The samples were analyzed with a scan rate of 3.0 °/min with a step size of 0.02 °. Neutron diffraction data were taken at Oak Ridge National Laboratory High Flux Isotope Reactor with the US/Japan wide-angle neutron diffractometer (WAND), with $\lambda = 1.48$ Å. Refinements for the x-ray data were done using the PDXL software package [21] and the ICSD database, and those for the neutron data were done using the FullProf program [22].

The x-ray diffraction spectra for all samples at room temperature are shown in Fig. 1. The neutron diffraction spectra at $T = 30$ K for $w = 0.7, 0.8, 1.0,$ and 1.1 and 10 K for $w = 0.9$ are shown in Fig. 2. Both x-ray and neutron powder diffraction confirm that the samples are predominantly LaCoO₃, with small amounts of crystalline Co₃O₄ phase. In most cases, the Co₃O₄ phase

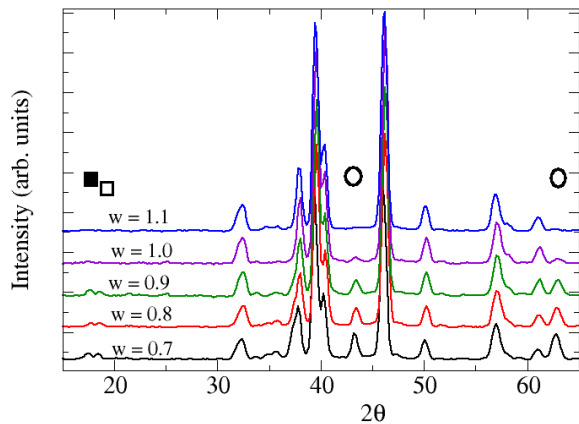


FIG. 2: Neutron diffraction spectra at wavelength $\lambda = 1.48\text{\AA}$ for $w = 0.7, 0.8, 1.0,$ and 1.1 and $T = 30$ K and for $w = 0.9$ at 10 K. The Co_3O_4 structural peaks are marked with an oval, the Co_3O_4 magnetic peak is marked with an empty box, and the CoO magnetic peak is marked with a filled box. The spectra are vertically offset for clarity.

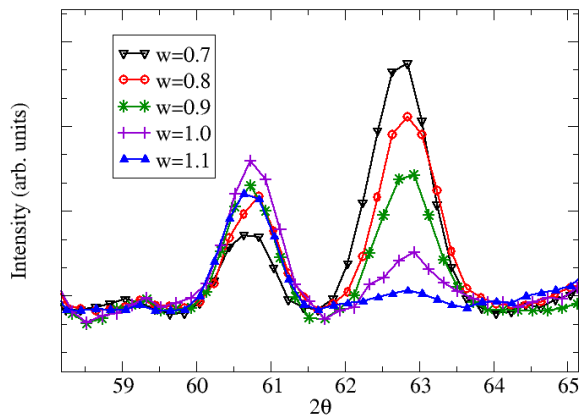


FIG. 3: LaCoO_3 (1 2 5) (left) and Co_3O_4 (4 4 0) (right) Bragg peaks at room temperature for all samples. The relative peak heights were used, along with the concentrations of Co_3O_4 in the other samples, to estimate the amount of Co_3O_4 in the $w = 1.1$ sample.

was included in refinements. Co_3O_4 Bragg peak intensities in the $w = 1.1$ sample were too small to include in either the x-ray or neutron refinements. This was also the case for the $w = 1.0$ x-ray data. Table I shows the weight percentage of Co_3O_4 in the samples as determined by the x-ray and neutron diffraction refinements where possible. Figure 3 shows the relative intensities of the LaCoO_3 (1 2 5) and Co_3O_4 (4 4 0) Bragg peaks, which were used to estimate the amount of Co_3O_4 in the $w = 1.1$ sample shown in Table I.

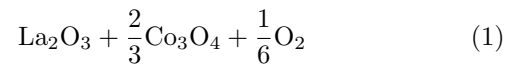
A magnetic Bragg peak corresponding to a CoO impurity phase is observed in neutron scattering scans for all samples below room temperature. This is to be expected, because Co_3O_4 can convert to CoO at temperatures above 900°C and the antiferromagnetic ordering

TABLE I: Calculated weight percentage of Co_3O_4 in each sample at room temperature determined using x-ray and neutron scattering data. The value for $w = 1.1$ is estimated using the relative intensities of peaks shown in Fig. 3.

w	% Co_3O_4 (neutron)	% Co_3O_4 (x-ray)
0.7	17.1(0.5)	20.3(1.2)
0.8	11.7(0.4)	11.8(0.8)
0.9	9.3(0.3)	7.4(0.8)
1.0	4.5(0.4)	—
1.1	2.4(0.4)	—

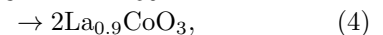
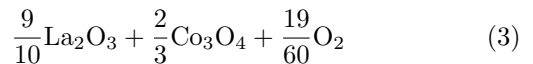
temperature of the latter is near 290 K [23]. The intensity of the CoO magnetic Bragg peak at $2\theta = 17.2^\circ$ is expected to be significantly larger than the CoO structural ones. Because structural peaks corresponding to CoO were not distinguishable in any of the scans, the CoO phase were not included in the structural refinements.

The formation of LaCoO_3 from La_2O_3 and Co_3O_4 requires oxygen supplied by the ambient atmosphere. For example, the most straightforward reaction would be

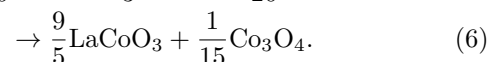
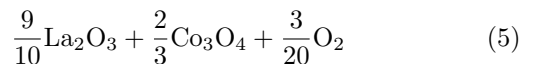


However, the presence of Co impurity phases seen in our $w = 1.0$ sample and in previous works on LaCoO_3 [17, 24] indicates that Eq. 1 does not fully describe reactions that are taking place. Likewise, the end products of other w samples do not strictly follow straightforward modifications of Eq. 1. Equation 1 significantly oversimplifies particle formation using the standard synthesis method described above.

As examples, two possibilities for the formation of a sample with a 10% deficiency of La_2O_3 might be envisioned. The first,



would result in a LaCoO_3 perovskite structure with La atoms missing from a significant number of sites. These vacant sites would be distributed randomly throughout the lattice, a scenario discussed by Androulakis *et al.* [25], and might be accompanied by localized structural distortions. The second possibility is the incomplete reaction of Co_3O_4 with La_2O_3 in which the LaCoO_3 phase forms, but crystalline Co_3O_4 remains in the sample,



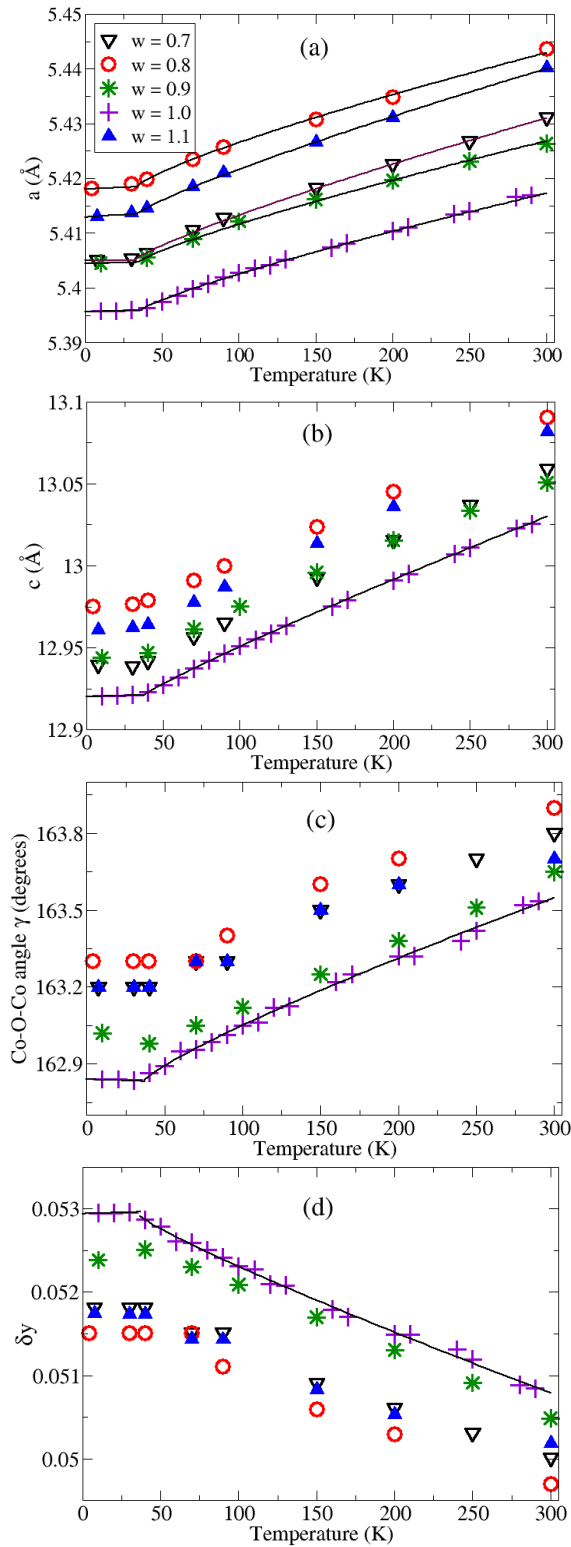
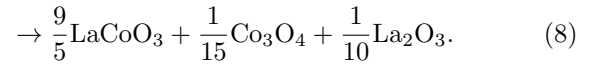
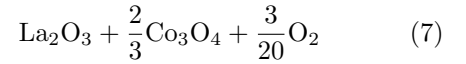


FIG. 4: Lattice parameters a (panel a), c (panel b), the Co-O-Co angle γ (panel c), and δy (panel d) for all samples as determined by neutron diffraction over a temperature range of 4 K to 300 K. Fits to power-law behavior for $T \geq T_0$ (Eq. 13) and to linear behavior for $T \leq T_0$ (Eq. 12) are shown for all samples in (a) and for the $w = 1.0$ sample in (b),(c), and (d). [17]

The two scenarios require different amounts of oxygen absorbed from the ambient atmosphere, with the second process requiring significantly less. If absorption of oxygen is a limiting factor, the second would be favored over the first.

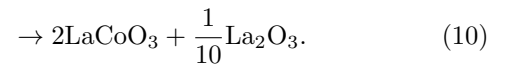
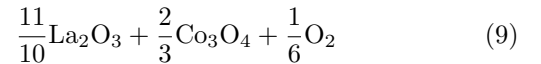
The observation of minor amounts of crystalline Co_3O_4 in our $\text{La}_{0.9}\text{CoO}_3$ sample indicates that the second scenario described in Eq. 5 might be the better description of the synthesis process for our particles. LaCoO_3 and $\text{La}_{1-x}\text{Sr}_x\text{CoO}_3$ powders are often synthesized [25–32] in an air atmosphere and are often described as being single phase as determined by x-ray diffraction. When the x-ray diffraction spectra are not shown, it is difficult to assess whether impurity phases are present. In a work where the spectra were provided, Ben Amor *et al.* [7], it was reported that varying the La:Co ratio resulted in essentially single phase LSCO with a small amount of CoO. However, the x-ray diffraction spectra exhibit small Bragg peaks corresponding to Co_3O_4 . As we have shown, minute Bragg peaks could represent magnetically significant amounts of crystalline Co_3O_4 . We will soon show that even small amounts of this phase can significantly affect the ferromagnetic behavior.

Our LaCoO_3 sample contains a small ($\approx 4.5\%$) amount of Co_3O_4 phase, which is consistent with insufficient oxygen absorption levels to allow complete conversion of the starting materials. An example of a reaction utilizing too little oxygen is



This process would result in a sample with 3.4% Co_3O_4 by weight. It must also contain La_2O_3 . However, no La_2O_3 Bragg peaks were observed using either x-ray or neutron diffraction. It is possible that very small (≤ 10 nm) nanoparticles of La_2O_3 form, which would result in broad, low intensity peaks difficult to see in the diffraction spectra. The La_2O_3 might also be amorphous.

We examined the effects of an excess La_2O_3 phase in the starting materials by synthesizing a sample with $w = 1.1$, *i.e.* 10% excess La. One possible reaction could be



However, although small amounts of Co_3O_4 and CoO phases are indicated by the Bragg peaks observed in the $w = 1.1$ powder, as in the other samples no crystalline La_2O_3 phase is observed. This indicates that the actual growth process is likely not homogeneous, as Eq. 9 would imply. Inhomogeneous growth processes might produce

TABLE II: Fit parameters for fits to the La_wCoO_3 lattice parameters shown in Fig. 4. Fits to a were done for all samples, while the fits to c , γ , and δy are shown for $w = 1.0$ from a previous work. [17] Fits to a were done using the equations $a(T) = a_0 + K_a(T - T_0)^\sigma$ ($T \geq T_0$) and $a(T) = a(0) + \alpha_a T$ ($T \leq T_0$), and similar equations were used for c , γ , and δy . The parameters K_x and α_x are in units of 10^{-4} ($[x]/\text{K}$) and 10^{-6} ($[x]/\text{K}$), respectively, where x is the relevant lattice parameter and $[x]$ are the relevant units.

	w	K_a	T_0 (K)	σ	$a_0(\text{\AA})$	$a(0)$ (\AA)	α_a
a	1.1	2.30(1)	34(3)	0.85(2)	5.4135(1)	5.4129(1)	18.4(1)
	1.0	2.08(1)	37(2)	0.83(2)	5.3960(1)	5.3956(1)	9.59(1)
	0.9	2.15(1)	35(3)	0.83(2)	5.4047(1)	5.4044(1)	7.97(1)
	0.8	2.80(1)	34(3)	0.80(2)	5.4185(1)	5.4180(1)	13.3(1)
	0.7	2.37(1)	32(3)	0.84(2)	5.4050(1)	5.4050(1)	0.00(1)
	w	K_c	T_0 (K)	σ	$c_0(\text{\AA})$	$c(0)$ (\AA)	α_c
c	1.0	7.02(1)	37(2)	0.91(2)	12.9206(1)	12.92(1)	33.7(1)
	w	K_γ	T_0 (K)	σ	$\gamma_0(\text{\AA})$	$\gamma(0)$ (\AA)	α_γ
γ	1.0	66.1(1)	37(2)	0.84(1)	162.835(1)	162.84(1)	200(1)
	w	$K_{\delta y}$	T_0 (K)	σ	$\delta y_0(\text{\AA})$	$\delta y(0)$ (\AA)	$\alpha_{\delta y}$
δy	1.0	-0.1558(1)	37(2)	0.88(1)	0.05291(2)	0.05294(2)	0.629(1)

local regions with conditions favoring the formation of Co_3O_4 .

Figure 4 shows the rhombohedral lattice parameters a (panel a) and c (panel b) as determined from neutron diffraction refinements, as well as the Co-O-Co angle γ (panel c) and δy (panel d). For the $w = 1.0$ powder, neutron scattering data were obtained for more temperatures and with longer counting times. As a result, there are improved statistics for data obtained with this sample relative to the other powders. The LaCoO_3 structure is a rhombohedrally distorted perovskite ($R\bar{3}c$ structure), where the Co^{3+} cations are octahedrally coordinated with the O^{2-} anions. In a cubic system, the Co-O-Co angle γ is 180° . However, in LaCoO_3 , the oxygen octahedra are twisted in order to accommodate the rhombohedral distortion, and γ is closer to 163° . [33] The parameter δy is a measure of the oxygen anion's deviation from the straight line connecting two neighboring Co cations, thereby quantifying the amount of distortion from cubic. [17, 34, 35] Mathematically,

$$\delta y = \frac{d}{a} \cos(\gamma/2) \quad , \quad (11)$$

where d is the Co-O bond length and a is the rhombohedral lattice parameter. [13] In these data, the a and c lattice parameters, γ , and δy all show similar temperature dependencies. Since d varies by less than 0.5 % over the entire range $5 < T < 300$ K, γ and δy are nearly proportional and essentially equivalent when characterizing the rhombohedral distortion and associated magnetic behavior. Both parameters have been used previously [13, 17] so we include both in our discussions.

Interestingly, the lattice parameters do not vary monotonically with the amount of Co_3O_4 phase. The $w = 1.0$

behavior represents the smallest values in the average lattice parameters a , c , and γ , and the largest value of δy for all T . Aside from the vertical shift of data in Fig. 4, Co_3O_4 does not greatly affect the shape of the lattice parameters vs T .

Fits to the a lattice parameter are shown for all samples in Fig. 4(a). The fits to the $w = 1.0$ data were reported previously [17] and are shown here for the c , γ , and δy lattice parameters as well (Fig. 4(b), (c), and (d)). In the previous work, it was shown that power law behavior describes the behavior of the parameters above $T_0 = 37(2)$ K, while a linear, nearly constant, behavior describes the parameters below T_0 . The lattice parameter $a(T)$ is thus well modeled by

$$a(T) = a(0) + \alpha_a T \quad (T < T_0) \quad (12)$$

and

$$a(T) = a_0 + K_a(T - T_0)^\sigma \quad (T > T_0). \quad (13)$$

The quantity a_0 is the value of a at T_0 , while α_a and K_a (units of $\text{\AA}/\text{K}$) are tunable coefficients. Similar equations were used to fit the c , γ , and δy lattice parameters for $w = 1.0$. Fitted parameters for Fig. 4 (a) through (d) are all given in Table II. For $w = 1.0$, the fits done using Eq. 13 were found to be significantly better than fits done based on the Gruneisen formulation using the Einstein model for specific heat. [9, 17, 36] Unlike the Gruneisen fits, the power law fits are able to account for the sharp increase in slope near T_0 and the negative curvature for $50 \leq T \leq 300$ K. Similar qualitative behavior can be seen in the $w \neq 1.0$ samples; they are also well fit by the power law. Although Radaelli *et al* fit their lattice parameters in the context of thermal excitations, it is difficult to

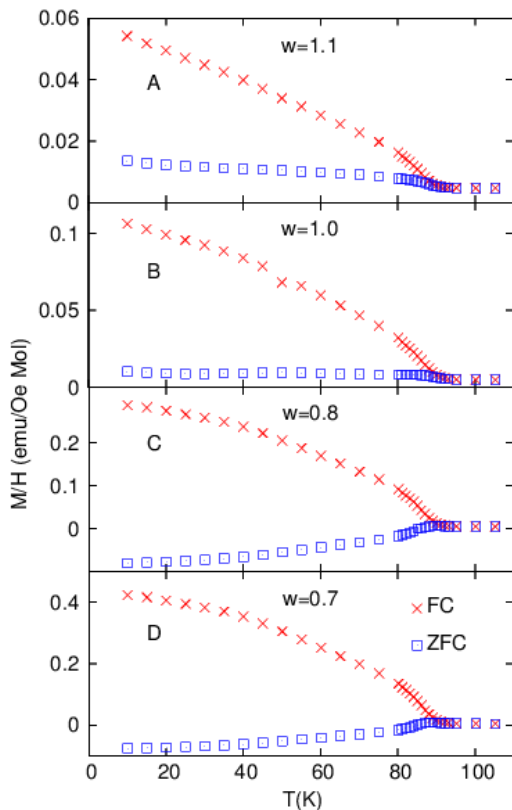


FIG. 5: ZFC and FC data for M/H vs T with $H = 20$ Oe for $w = 1.1$ (A), 1.0 (B), 0.8 (C), and 0.7 (D).

assess those fits in the range we are examining because of the sparse temperature sampling. [33] In addition, the fits described are in the context of a Jahn-Teller distortion; as was previously discussed, a significant such effect has not been found in these materials.

The power law fits we propose imply a phase transition at T_0 that is expressed in the lattice parameter a for all w . As can be seen for the $w = 1.0$ sample, the same T_0 has been used successfully for all of the lattice parameters. [17] The exponent σ gave the best fit for the range $0.80 \leq \sigma \leq 0.85$ across the samples. During the fitting procedure, a range of $32 \leq T_0 \leq 37$ K was found to give the best fit, with all samples $w \neq 1.0$ exhibiting a lower value than that for $w = 1.0$. However, as the temperature sampling was only done every 10 K, further experiments would be required to determine T_0 more accurately for $w \neq 1.0$. Nonetheless, the behavior of the other samples appears similar to that of $w = 1.0$, but with small vertical offsets.

Magnetometry

The field-cooled (FC) and zero-field-cooled (ZFC) magnetizations were measured in applied fields $20 < H < 5000$ Oe for $10 \leq T \leq 110$ K using Quantum Design

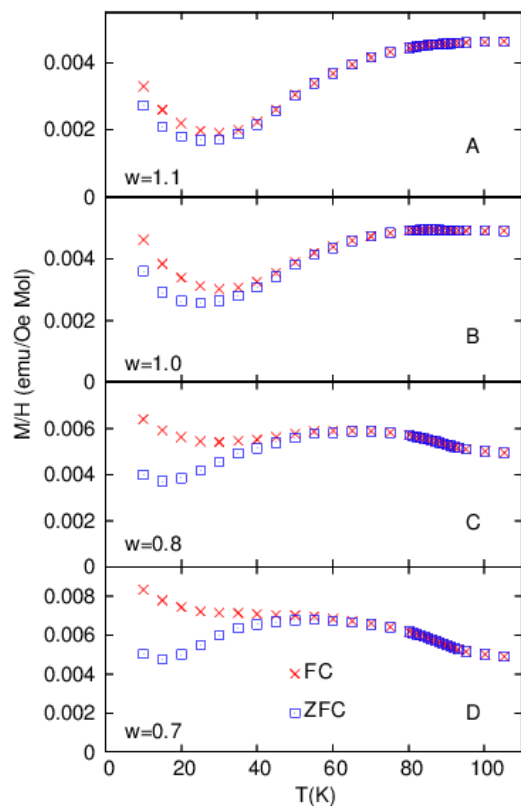


FIG. 6: ZFC and FC data for M/H vs T with $H = 5000$ Oe for $w = 1.1$ (A), 1.0 (B), 0.8 (C), and 0.7 (D).

SQUID magnetometers. M/H vs T is shown for $w = 1.1$, 1.0, 0.8, and 0.7 in Fig. 5 and Fig. 6 for $H = 20$ and 5000 Oe, respectively. For $H = 20$ Oe, a sudden increase in magnetization indicating ferromagnetic ordering is evident upon FC. The critical temperature for this ordering is $T_C = 88.5 \pm 0.5$ K for $w = 1.1$ and $T_C = 89.5 \pm 0.5$ K for $w = 1.0$, 0.8, and 0.7. The ZFC magnetization remains small compared to FC below T_C and likely indicates metastable domain structure which is frozen in as the sample is cooled. These ZFC domains are not eliminated until T approaches T_C . A slight difference between FC and ZFC data is observed for temperatures $T_C < T < 92$ K, which reflects rounding of the transition. This could result from inhomogeneities in the system and from the applied field limiting the approach to the zero-field ferromagnetic critical point.

For $H = 5000$ Oe, the difference between FC and ZFC is smaller than for 20 Oe and increases with the amount of Co_3O_4 . Ferromagnetic long-range ordering is not apparent at this field. One prominent feature of M/H vs T is a ZFC minimum in M/H vs T near $T = 20$ K that becomes more subdued as the Co_3O_4 concentration increases. The tendency towards a minimum is weaker for FC, particularly for the $w = 0.7$ and 0.8 powders. For other values of H between 20 and 5000 Oe, the behaviors appear intermediate, as expected. The size of the

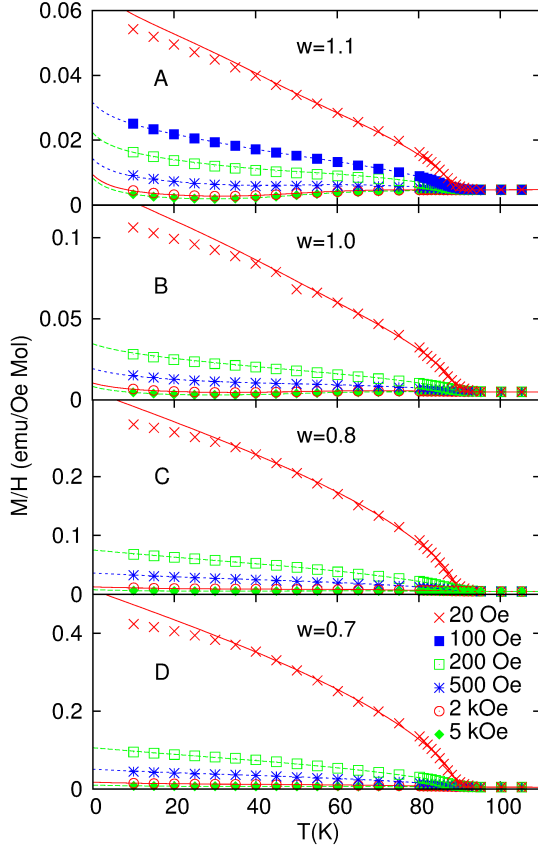


FIG. 7: M/H vs T upon FC for La_wCoO_3 with $w = 1.1, 1.0, 0.8$ and 0.7 in applied fields $20 < H < 5000$ Oe.

net moment attributed to ferromagnetic ordering and the difference between the FC and ZFC magnetizations both increase with the Co_3O_4 concentrations, indicating that they are a direct consequence of this impurity phase.

Figures 7 and 8 show FC data for M/H vs T and H/M vs T , respectively, for six different applied fields ($H = 20, 100, 200, 500, 2000$, and 5000 Oe). Well above T_C , the behavior appears approximately linear, indicating a paramagnetic Curie-Weiss contribution for all samples. For $w = 1.0$, the best fit to the Curie-Weiss behavior for the range $170 < T < 300$ K,

$$H/M = \frac{T + \theta_{CW}}{C}, \quad (14)$$

was done elsewhere [17] and yielded values $C = 1.49 \pm 0.02$ emu-K/mol and $\theta_{CW} = 182 \pm 4$ K. The Curie-Weiss expression gives $H/M = 122 \pm 4$ Oe-mol/emu at $T = 0$. Normally, one would not expect to be able to extrapolate to $T = 0$, because a transition to antiferromagnetic long-range order is expected at a temperature on the order of θ_{CW} , and correlated behavior is expected to occur well above that. If the behavior followed the straight line indicated by Curie-Weiss, the implication would be

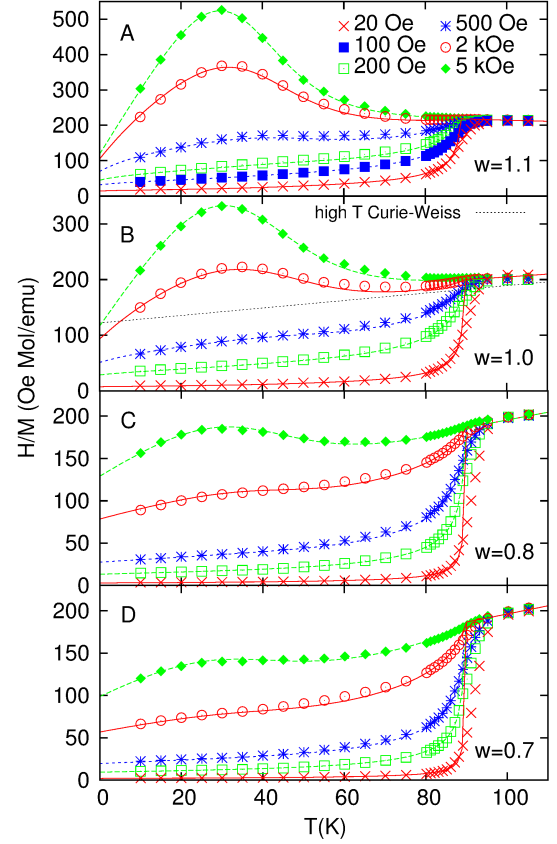


FIG. 8: H/M vs T upon FC for La_wCoO_3 with $w = 1.1, 1.0, 0.8$ and 0.7 in applied fields $20 < H < 5000$ Oe. The straight line in panel B is the Curie-Weiss fit [17] for $150 < T < 300$ K.

that correlations remain short-ranged. Indeed, the broad peak in H/M near 30 K for all samples at $H = 2$ and 5 kOe indicates significant antiferromagnetic correlations, although the peak is much too broad to indicate an antiferromagnetic transition for $T > 5$ K.

The data shown in Figs. 7 and 8 indicate that there are both ferromagnetic and antiferromagnetic correlations in this system. Whereas ferromagnetic long-range order is apparent near T_C at low fields, at high fields the system exhibits paramagnetic behavior with antiferromagnetic correlations. A fit of the FC data combining one type of paramagnetic behavior and a transition to long-range ferromagnetic order for smaller fields proved inadequate. In particular, the broad peak for high fields in H/M vs T , where the contribution from ferromagnetic long-range order is very small, is not well characterized by a single paramagnetic-like function. Instead, for $w = 1.1, 1.0, 0.8$ and 0.7 , we were able to fit the FC data to the function

$$\frac{M(T)}{H} = \left(d + \frac{E_a}{T + t_a}\right)S(T) + \left(\frac{E_b}{T + t_b}\right) + M_n \left(\frac{T_c - T}{T_c}\right)^\beta (S(T) + L(1 - S(T))), \quad (15)$$

for $T \leq T_C$ and

$$\frac{M(T)}{H} = \left(d + \frac{E_a}{T + t_a}\right)S(T) + \left(\frac{E_b}{T + t_b}\right) \quad (16)$$

for $T \geq T_C$. The first and third terms of Eq. 15, along with the first term of Eq. 16, are modified by a sigmoid. The sigmoid is characterized by an inflection point at a temperature T_S and an inverse width W ,

$$S(T) = \frac{1}{1 + \exp(W(T_S - T))}. \quad (17)$$

Equation 15 consists of three contributions to the magnetization. The first two terms represent paramagnetic behaviors parameterized by Curie-Weiss-like expressions, while the power law behavior in the third term represents ferromagnetic long-range ordering below the transition temperature T_C . The sigmoid function modifies the first term, $E_a/(T + t_a)$, and characterizes a reduction of the high temperature paramagnetism over a temperature range parameterized by W and centered at a temperature T_S . The second term, $E_b/(T + t_b)$, represents the low T paramagnetic behavior that exists even when the high temperature paramagnetic behavior has disappeared. These functions work well over the temperature range $T \leq T_C$. However, E_a and t_a differ from the paramagnetic behavior for $T > 170$ K because significant antiferromagnetic correlations have built up for $T < 110$ K. Similarly, E_b and t_b should not be interpreted in the usual way for Curie-Weiss behavior because the correlations are not necessarily negligible over this region of the fit. The expression should be considered a convenient approximation for fitting the data. The quantity M_n is a field dependent coefficient for the ferromagnetic behavior, where n indicates the field in Oe. β is the power-law exponent. The parameter L allows for a slight variation of the power law magnitude as the decreasing temperature approaches T_S and improved fits for $w = 1.0$ and 1.1.

The fits of the FC data to Eq. 15 and 16 are shown in Fig. 7 and 8. The parameters obtained are given in Table III. Although the fitted curve at each field involves a large number of parameters, it should be noted that the only parameter that is allowed to vary with field is M_n . Hence, the fits are well constrained by the data at the several fields used. The ferromagnetic order is most evident for $H = 20$ Oe in the M/H vs T behavior shown in Fig. 7. For H/M vs T , shown in Fig. 8, the high field

TABLE III: Fit parameters for samples $w = 1.1, 1.0, 0.8,$ and 0.7 using Eq. 15, 16 and 17 with fixed value $\beta = 0.63$. The subscript n in M_n refers to the applied field in Oe. Error estimates are indicated in the $w = 1.0$ column and are similar for the other powders except where indicated.

	Units	$w=1.1$	$w=1.0$	$w=0.8$	$w=0.7$
T_C	(K)	88.5	89.5(5)	89.5	89.5
W	(1/K)	0.11	0.09(1)	0.09	0.09
T_S	(K)	47(2)	49(2)	45(3)	40(3)
t_a	(K)	180	180	180	180
t_b	(K)	6.5	11.5(5)	40	35(5)
E_a	($\frac{\text{emu}\cdot\text{K}}{\text{mol}\cdot\text{Oe}}$)	-0.82	0.60(2)	0.86	0.85
E_b	($\frac{\text{emu}\cdot\text{K}}{\text{mol}\cdot\text{Oe}}$)	0.054	0.094(1)	0.29	0.28(1)
L	-	1.25	1.2(2)	1	1
d	($\frac{\text{emu}}{\text{mol}\cdot\text{Oe}}$)	0.0071	0.0019(2)	0.00	0.0
M_{20}	($\frac{\text{emu}}{\text{mol}\cdot\text{Oe}}$)	0.048	0.106(3)	0.337	0.503
M_{100}	"	0.187	-	-	-
M_{200}	"	0.0112	0.022(2)	0.068	0.098
M_{500}	"	0.0048	0.0092(3)	0.029	0.043
M_{2000}	"	0.0009	0.0018(2)	0.0055	0.0095
M_{5000}	"	0.0000	0.0000(1)	0.0005	0.002

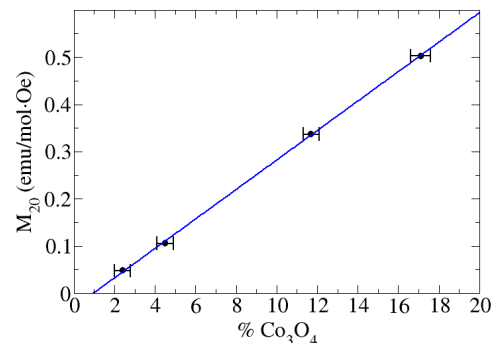


FIG. 9: The fitted value of M_{20} (see Table III) vs the weight percentage of Co_3O_4 for $w = 0.7, 0.8, 1.0,$ and 1.1 (see Table I). Weight percentages are taken from the neutron scattering only. The data are well fit with a straight line.

behavior is most obvious and the ferromagnetic order is difficult to discern. A good fit for each sample requires that the fits for every H be of high quality; this is not necessarily a simple task, as the behavior of M/H is notably different at high and low fields. Data very close to T_C are extremely difficult to fit given the rounding of the transition, which can be seen in Fig. 7. The paramagnetism is not directly affected by the ferromagnetic long-range order, as is evident from the additive nature of the two behaviors.

The magnitude of the power law characterizing the ferromagnetic long-range order increases with the concentration of Co_3O_4 . Figure 9 shows the parameter M_{20} , which describes the magnitude of the order parameter for $H = 20$ Oe, vs the concentration of Co_3O_4 , determined from neutron scattering and listed in Table I. The results are consistent with a linear proportionality, as shown in Fig. 9. This behavior indicates that the ferromagnetic

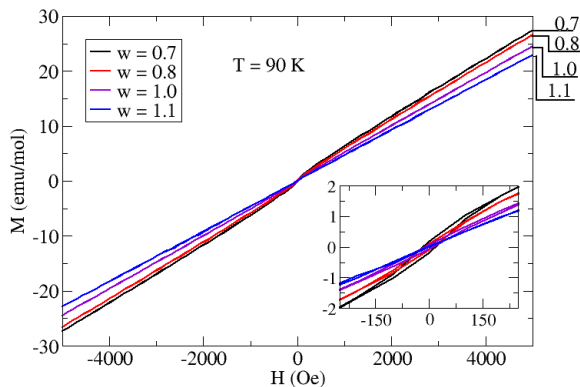


FIG. 10: M vs H for $w = 1.1, 1.0, 0.8$ and 0.7 at $T = 90$ K in an applied field $-5 < H < 5$ kOe. Inset shows the small amount of hysteresis for near $H = 0$.

long-range order is associated with the Co_3O_4 particles. If the Co_3O_4 particles are of similar size and shape in each of the samples, the proportionality is consistent with the amount of $\text{Co}_3\text{O}_4/\text{LaCoO}_3$ interface area. The increase in the ferromagnetic moment at T_C cannot be associated with the Co_3O_4 particles ordering magnetically, as their antiferromagnetic ordering temperature is between 25 and 40 K. [23]

Further evidence that the ferromagnetism originates within the interfaces, and that its critical behavior is dominated by ordering *near* the interfaces, comes from the order parameter critical exponent β . Normally, in three dimensions ($D = 3$), the bulk order parameter exponent would be close to a value $1/3$, much less than the mean field result $\beta = 1/2$. In the case of the ferromagnetism seen in the bulk particles, $\beta = 0.63 \pm 0.02$ is clearly greater than the mean field exponent. However, this value is consistent with the exponent predicted by Binder and Hohenberg for surface magnetic ordering, [37, 38] which strongly suggests that the ferromagnetism is associated with the surfaces of the particles and interfaces with impurity phases. Surface ordering is normally assisted by and masked by the $D = 3$ bulk ordering. In our case, while the surfaces order ferromagnetically, the interior is dominated by the antiferromagnetic interactions and never orders. This allows the ferromagnetic signal to be readily observed, but begs the question of how the surface ordering can take place. It is possible that in the interface region, antiferromagnetic ordering takes place but supports the ferromagnetism via canting of the spins. Another possibility is that the antiferromagnetic interactions support the surface ordering even though antiferromagnetic long-range ordering never takes place.

The magnetization curves for $w = 0.7, 0.8, 1.0$ and 1.1 as a function of the applied field at temperatures $T = 90, 70,$ and 40 K are shown in Figs. 10, 11 and 12, respectively (note that different figures have differ-

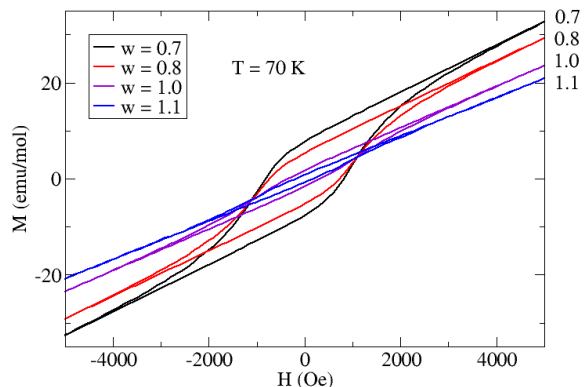


FIG. 11: M vs H for $w = 1.1, 1.0, 0.8$ and 0.7 at $T = 70$ K in an applied field $-5 < H < 5$ kOe.

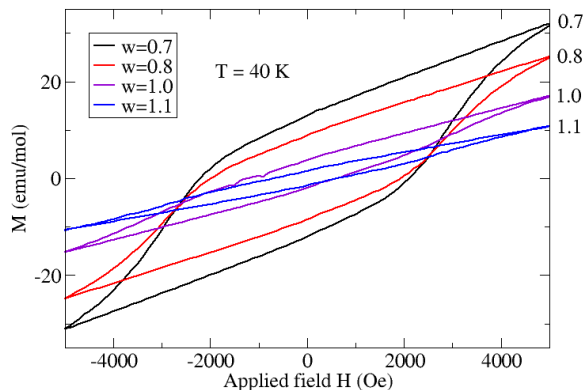


FIG. 12: M vs H for $w = 1.1, 1.0, 0.8$ and 0.7 at $T = 40$ K in an applied field $-5 < H < 5$ kOe.

ent vertical scales). Figure 13 shows similar data for $w = 0.7$ and 1.1 at $T = 10$ K. Figure 14 shows data for $w = 0.9$ and 1.0 at $T = 5$ K over an applied field of $-60 < H < 60$ kOe. The samples were ZFC to the measurement temperatures. The initial rise from $H = 0$ to the maximum field is not shown in order to increase the clarity of the plots. The values of $M(H = 0)$ and $H(M = 0)$ are given in Table IV.

At 90 K, all of the samples show a nearly linear response with little hysteresis, as would be expected above T_C . The hysteresis is more significant for $w = 0.7$ and 0.8 at $H = 0$, consistent with the larger ferromagnetic moment below T_C in these samples. The magnetization at $H = 5$ kOe increases by about 4.5 emu/mol as w decreases from 1.1 to 0.7, also consistent with a larger ferromagnetic moment as the amount of Co_3O_4 increases.

At $T = 70$ K, well below T_C , all samples show significant hysteresis (Fig. 11), while the coercive field $H(M = 0)$ and the remanent magnetization $M(H = 0)$ increase with the concentration of Co_3O_4 , as shown in Table IV. The samples with $w = 1.0$ and 1.1 show a smaller net magnetization at $H = 5$ kOe compared to the values at $T = 90$ K. In contrast, for $w = 0.8$ and 0.7 , the mag-

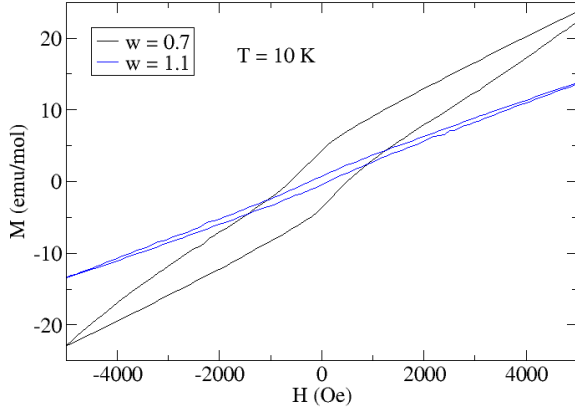


FIG. 13: M vs H for $w = 1.1$ and 0.7 at $T = 10$ K in an applied field $-5 < H < 5$ kOe. Inset shows the hysteresis for near $H = 0$.

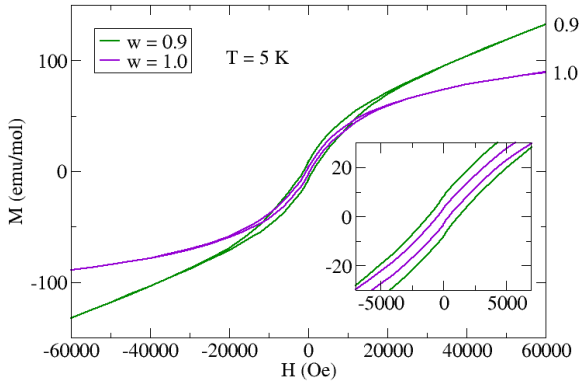


FIG. 14: M vs H for $w = 1.0$ and 0.9 at $T = 5$ K in an applied field $-60 < H < 60$ kOe. Inset shows the behavior near $H = 0$ more clearly.

TABLE IV: Values for $M(H = 0)$ and $H(M = 0)$ for the M vs H plots shown in Figs. 10 - 14. The + and - subscripts indicate whether the value was taken as H was decreased from its highest value (+) or increased from its lowest value (-). M is in emu/mol and H is in Oe.

T (K)	w	$M_+(H = 0)$	$M_-(H = 0)$	$H_+(M = 0)$	$H_-(M = 0)$
5	0.9	8.11	-8.14	1210	-1170
	1.0	3.25	-3.16	500	-410
10	0.7	4.36	-3.67	520	-620
	1.1	0.76	-0.45	190	-230
40	0.7	12.9	-12.1	2140	-2170
	0.8	8.83	-8.51	2020	-1940
	1.0	3.75	-1.95	670	-1130
	1.1	1.53	-1.49	740	-540
70	0.7	7.74	-7.65	820	-810
	0.8	5.28	-5.28	730	-730
	1.0	1.69	-1.67	330	-330
	1.1	0.77	-0.78	180	-180
90	0.7	0.18	-0.20	19	-17
	0.8	0.09	-0.12	13	-11
	1.0	0.07	-0.08	13	-12
	1.1	0.02	-0.018	3.6	-3.8

netization at $H = 5$ kOe is larger than the values at $T = 90$ K.

For $T = 40$ K, all of the samples exhibit hysteresis (Fig. 12) loops with a much greater enclosed area than for $T = 70$ and 90 K. The hysteresis loops extend to the maximum field applied, $|H| = 5$ kOe. The magnetization at 5 kOe is smaller than at higher temperatures for all samples. The difference in M between samples at $H = 5$ kOe is much greater at $T = 40$ K than at the higher temperatures, mainly a consequence of the decrease in M/H for the samples with less Co_3O_4 and the increase for those with more Co_3O_4 .

At $T = 10$ K, hysteresis persists to $H = 5$ kOe for both $w = 0.7$ and 1.1 (Fig. 13). However, the remanent magnetization in both cases is smaller relative to that at the higher temperatures: $M(H = 0)$ of $w = 1.1$ is half of its value at 40 K, and that of $w = 0.7$ is one third of its value at 40 K. Neither sample shows a tendency to saturate for $H < 5$ kOe.

It is clear from Table IV that the hysteresis loops increase as T decreases from $T = 90$ to 40 K, as one might expect as the ferromagnetic long-range order increases. However, it is unusual that the hysteresis then strongly decreases as T is reduced to 10 K. This is consistent with the behavior of M/H vs T in Fig. 7, where the ferromagnetism drops below the power law for $T < 40$ K.

The hysteresis in M vs H at $T = 5$ K was measured for $w = 1.0$ and 0.9 for $-60 \leq H \leq 60$ kOe. The $w = 1.0$ sample appears to be approaching saturation at high fields (Fig. 14), and $M(H = 60$ kOe) is 89.3 emu/mol. The hysteresis becomes negligible at 40 kOe and the remanent magnetization is only about 0.2 emu/mol larger than that in the sample at 40 K. The $w = 0.9$ sample does not appear to be saturating at 60 kOe, and $M(H = 60$ kOe) is 133 emu/mol. Although the remanent field is larger in this sample than in the $w = 1.0$ sample (8.1 emu/mol as compared to 3.3 emu/mol), the hysteresis is also nearly gone at 40 kOe. These data suggest that there are more ferromagnetically interacting moments available in the $w = 0.9$ sample relative to the 1.0 one, which is consistent with the larger interface region that accompanies the higher Co_3O_4 content.

Discussion

As can clearly be seen in Fig. 5 and 7, ferromagnetic long-range order is present for all w at low fields. From Fig. 9, it is clear that the magnitude of the ferromagnetic power law contribution increases linearly with the weight percentage of Co_3O_4 . For all samples, this ferromagnetic contribution is well-fit by the exponent $\beta = 0.63$ near T_C , strongly indicating surface/interface magnetism. [37, 38] Hence, the magnetic data are well modeled with ferromagnetic long-range order occurring primarily at the interfaces of LCO and Co_3O_4 .

At high fields, where the ferromagnetic long-range order is weak, the antiferromagnetic behavior dominates, as can be seen from Fig. 6 and 8 and Table III. The gentle increase in H/M just below T_C for $H = 5000$ Oe indicates that the antiferromagnetic correlations are increasing, as expected from the Curie-Weiss fit for $T \geq 170$ K yielding $\theta_{CW} = 182$ K. However, there is no indication of a sharp phase transition to long-range antiferromagnetic order. Instead, H/M vs T shows a very broad peak near $T = 30$ K. The decrease in H/M below this temperature appears to indicate a weakening of the antiferromagnetic correlations. In general, antiferromagnetic behavior becomes more apparent in the magnetization plots as the Co_3O_4 amount decreases - this is even more obvious in the single crystal data of Yan *et al.*, [39] where M/H shows a steep dropoff for $T < T_C$. Single crystals likely contain very little Co_3O_4 due to the synthesis process.

At $T = 0$, the extrapolated value of H/M is near the extrapolated value from the Curie-Weiss fit for $170 < T < 300$ K. Although possibly coincidental, this may suggest that the antiferromagnetic correlations at $T = 0$ are insignificant, because the high T Curie-Weiss behavior only holds where correlations between spins are insignificant. The lack of a transition to antiferromagnetic long-range order and the possibility of negligible antiferromagnetic correlations at $T = 0$ suggest that the antiferromagnetic interactions are frustrated at low T .

The experimental data and the fits performed on the magnetization plots show that there exists both ferromagnetic long-range ordering and antiferromagnetic correlations in La_wCoO_3 . The fits to the behavior shown in Fig. 8 and Table III indicate that the ferromagnetic and antiferromagnetic behaviors do not interact significantly. These findings are consistent with data from other studies [25, 39–41]; what remains unclear, however, is the microscopic origin of these behaviors.

Thin film studies [16, 18, 40] have suggested that LCO thin films grown on certain substrates exhibit ferromagnetic long-range order, in particular when the substrate induces tensile stress at the interface with LCO. Sterbinsky *et al* reported that a 20 nm film of LCO deposited on a SrTiO_3 (STO) substrate had a significantly elongated in-plane Co-O bond length and a shortened out-of-plane bond length compared to the bulk value. [18] They estimated Co-O-Co angles of 168° and 159° for the in- and out-of- plane bond lengths, respectively. Another thin film study by Fuchs *et al* connected structural distortions to the presence of ferromagnetic order, estimating that the Co-O-Co angle above which there can be ferromagnetism is approximately 160° . [16, 40] All of our data show Co-O-Co angles well above this value, with the minimum angle seen at 162.8° .

Knizek *et al.*, in a more localized spin-state approach, discussed how the strong hybridization between the Co e_g states and the O p states might lead to the presence of spins in the nominally higher energy magnetic state. [42]

This hybridization corresponds to a larger Co-O-Co angle, a longer Co-O bond length, and a lower amount of rhombohedral distortion (smaller δy). Lee and Harmon, using an extended state GGA calculation, found that for $\delta y = 0.052$ the magnetic state is only 3.2 meV/Co higher in energy than a nonmagnetic state. [13] They suggested that even small distortions in the lattice or thermal energy could be enough to allow a magnetic state. As δy decreases, the minimum in the energy plot shifts to favor a magnetic state more strongly. Seo *et al* found in their theoretical calculations that tensile stress can induce ferromagnetically interacting spins on some Co ions at the film/substrate interface. [15] The importance of tensile stress in inducing long-range ferromagnetic order is most convincingly demonstrated by the spintronic device discussed in Hu *et al.* [20] By growing a thin film of LCO on a substrate of SrTiO_3 , the piezoelectric property of the substrate can be used to apply tensile stress to the LCO film to induce ferromagnetism.

It is clear from these studies that the rhombohedral distortion and tensile stress play crucial roles in the magnetic behavior of LCO. In our particles, the near proportionality of the amount of Co_3O_4 and the strength of the ferromagnetic ordering, as well as the 2D nature of the critical exponent, strongly suggest that ferromagnetism is associated with the interface regions and these regions are a source of tensile strain. The extensive work performed by Yan *et al* on one sample of LCO with different surface areas ranging from a single crystal to nano-sized powder demonstrated that the *surface* of LCO can also be a source of tensile strain and ferromagnetic long-range order. [39]

A comprehensive model of the magnetic behavior in LCO must account for the phenomena discussed above, namely the surface/interface ferromagnetism and the unusual temperature dependence of the antiferromagnetic correlations, including the apparent weakening of these correlations below a certain temperature.

Although the ferromagnetic ordering is associated with the interface region, it may well propagate into the LCO particles to a significant depth. Fuchs *et al* found that highly stressed LCO films exhibited a decreasing ferromagnetic order to depths of 100 nm when deposited on $(\text{LaAlO}_3)_{0.3}(\text{SrAl}_{0.5}\text{Ta}_{0.5}\text{O}_3)_{0.7}$ (LSAT) substrates. [40] Other experiments indicate ferromagnetism persisting for 20 to 30 nm into LCO [18, 20], while experiments on nanoparticle LCO suggest it is in the range of 20 - 100 nm. [43, 44] Based on these studies, we roughly estimate that ferromagnetism penetrates our particles to a depth of 20 to 100 nm.

A significant part of the bulk samples exhibit paramagnetism with net antiferromagnetic interactions but with no antiferromagnetic long-range order down to our lowest measuring temperature, $T = 5$ K. Furthermore, the correlations appear to diminish as T decreases below 30 K. Calculations indicate that δy correlates with

the magnetic state and suggest the existence of a critical value near $\delta = 0.052$, [13] very close to the critical value $\delta y = 0.053$ found for $w = 1.0$. This critical value is achieved just below T_0 . Just above it, δy and all other lattice parameters exhibit a power law behavior in $T - T_0$, which has been said to indicate a phase transition. [17]

To address all of these phenomena we consider a core-interface model consisting of two regions, not necessarily sharply delineated or having boundaries that are temperature independent. The model addresses all of the observed behaviors listed above. The *core* region describes the particle interiors far from surfaces and interfaces with Co_3O_4 , while the *interface* region consists of LCO in close proximity to the surfaces and interfaces. The surfaces and interfaces impose tensile strain throughout the latter region. Particles with fewer surfaces, fewer defects that act like surfaces, and fewer interfaces with impurity phases will have relatively small amounts of the interface region and more core region. Note that the model does not address the *details* of the interactions, which we believe are better addressed by band structure calculations and experiments such as x-ray absorption and are thus beyond the scope of this paper.

We first discuss the interface region. The LCO material near the surfaces and interfaces is strained in a manner similar to that in the thin films [16, 40] and nanoparticles [44] in previous studies, all of which exhibit a ferromagnetic transition at $T_C \approx 90$ K. The particle size in our bulk materials is essentially the same throughout all of the samples, as indicated by the identical synthesis methods and by the lack of variation in peak width for the neutron and x-ray scattering data. The variation in the amount of ferromagnetism must therefore be due to Co_3O_4 in the samples, the crystallites of which form interfaces with the LCO during synthesis. Co_3O_4 is an antiferromagnetic material with $T_N \approx 40$ K [23], far removed from the LCO T_C . Hence, it is the structural strain and not the magnetic ordering of the Co_3O_4 that enhances the ferromagnetism in LCO, in the same manner as a particle surface or a thin film substrate. Furthermore, the tensile strain in the interface region must extend into the LCO bulk, much like the strain from a substrate extends into the LCO thin film. Given the significant thermal expansion of LCO (as seen in the lattice parameters, Co-O-Co angle, and δy), the extent of this strain may be affected by the contraction of the lattice as the material cools; LCO bulk material in between the core and interface regions likely experiences a variation in strain with temperature which results in changing magnetic correlations.

In contrast to the interface region, the core region is dominated by antiferromagnetic interactions, but never exhibits long-range order. These interactions are strongly affected by the lattice contraction with temperature, as can be seen with the rhombohedral distortion parameter. δy increases with a power law behavior as T decreases,

until a critical value of δy between 0.051 and 0.053 is reached at $T_0 \approx 40$ K. Below T_0 , the change is δy is relatively small. The transition is observed for all values of w studied, although the average δy is smaller for larger Co_3O_4 concentrations. Keeping in mind that the values for these lattice parameters are averaged over the entire particle, the variation in the low T value of δy across samples can be attributed to the rhombohedral distortion in the interface region remaining smaller than in the core region as a possible consequence of tensile strain. As such, only the core material will reach the critical value of δy , at which a magnetic state is not energetically favorable.

Conclusion

In conclusion, we have shown that the LaCoO_3 phase is robust even in the presence of non-stoichiometric starting materials, and that it is unlikely that significant amounts of La-deficient unit cells are forming. Instead, the excess Co_3O_4 introduced remains in the sample in crystalline form and allows for LCO/ Co_3O_4 interfaces to form.

We introduce an interface-core model as a novel rationalization for the magnetic behavior in bulk La_wCoO_3 . The core LCO material far from the interfaces is paramagnetic with antiferromagnetic correlations, and does not order despite a large Curie temperature; this is due at least in part to a shift into a non-magnetic state as a result of the system reaching a critical value of δy as T decreases. However, the LCO material near the surfaces and interfaces with Co_3O_4 experiences tensile strain - this region is thus prevented from reaching the critical value of δy , and in fact exhibits ferromagnetic order with $T_C \approx 90$ K, consistent with the findings of thin film studies. Studies such as band structure calculations and x-ray absorption experiments are needed to further address the magnetic correlations in the core regions above and below T_0 , as well as the strain mechanism for inducing ferromagnetic long-range order in the interface regions.

We also present a phenomenological model for the magnetization of La_wCoO_3 which is consistent with the behavior over a range $20 \text{ Oe} \leq H \leq 5 \text{ kOe}$, and which also fits the inverse magnetization. By modifying Curie-Weiss behavior with a sigmoid, and by including a ferromagnetic power-law behavior with an exponent indicating surface magnetism, we show that the system possesses both antiferromagnetic correlations and ferromagnetic order. Further calculations will ideally simplify the mathematical model and further elucidate the origin of the sigmoid-type behavior.

We thank F. Bridges, A. M. Coogan, A. Elvin, B. Harmon, and S. Shastry for helpful discussions and/or assistance with measurements. The work at the High Flux Isotope Reactor at ORNL was supported by the DOE BES Office of Scientific User Facilities. Work at Lawrence Berkeley National Laboratory was supported

by the Director, Office of Science (OS), Office of Basic Energy Sciences (OBES), of the U.S. Department of Energy (DOE) under Contract No. DE-AC02-05CH11231.

-
- [1] M. A. Korotin, S. Y. Ezhov, I. V. Solovyev, V. I. Anisimov, D. I. Khomskii, and G. A. Sawatzky, *Phys. Rev. B* **54**, 5309 (1996).
- [2] J. B. Goodenough, *J. Phys. Chem. Solids* **6**, 287 (1958).
- [3] M. A. Senaris-Rodriguez and J. B. Goodenough, *J. Sol. State Chem.* **116**, 224 (1995).
- [4] D. Louca and T. Egami, *Phys. Rev. B* **59**, 6193 (1999).
- [5] P. Phelan, D. Louca, K. Kamazawa, M. F. Hundley, and K. Yamada, *Phys. Rev. B* **76**, 104111 (2007).
- [6] I. Fita, V. Markovich, D. Mogilyansky, R. Puzniak, A. Wisniewski, L. Titelman, L. Vradman, M. Herkowitz, V. Varyukhin, and G. Gorodetsky, *Phys. Rev. B* **77**, 224421 (2008).
- [7] A. B. Amor, M. Koubaa, W. Cheikhrouhou-Koubaa, and A. Chiekhrouhou, *J. Alloys and Comp.* **457**, 1 (2008).
- [8] M. Itoh, I. Natori, S. Kubota, and K. Motoya, *J. Phys. Soc. Jpn.* **63**, 1486 (1994).
- [9] R. Caciuffo, D. Rinaldi, G. Barucca, J. Mira, J. Rivas, M. A. Senaris-Rodriguez, P. G. Radaelli, D. Fiorani, and J. B. Goodenough, *Phys. Rev. B* **59**, 1068 (1999).
- [10] Y. Jiang, F. Bridges, N. Sundaram, D. P. Belanger, I. E. Anderson, J. F. Mitchell, and H. Zheng, *Phys. Rev. B* **80**, 144423 (2009).
- [11] N. Sundaram, Y. Jiang, I. E. Anderson, D. P. Belanger, C. H. Booth, F. Bridges, J. F. Mitchell, T. Proffen, and H. Zheng, *Phys. Rev. Lett.* **102**, 026401 (2009).
- [12] S. Medling, Y. Lee, H. Zheng, J. F. Mitchell, J. W. Freeland, B. N. Harmon, and F. Bridges, *Phys. Rev. Lett.* p. 157204 (2012).
- [13] Y. Lee and B. N. Harmon, *J. Appl. Phys.* **113**, 17E145 (2013).
- [14] V. Krapek, P. Novak, J. Kunes, D. Novoselov, D. M. Korotin, and V. I. Anisimov, *Phys. Rev. B* **86**, 195104 (2012).
- [15] H. Seo, A. Posadas, and A. A. Demkov, *Phys. Rev. B* **86**, 014430 (2012).
- [16] D. Fuchs, E. Arac, C. Pinta, S. Schuppler, R. Schneider, and H. v. Lohneysen, *Phys. Rev. B* **77**, 014434 (2008).
- [17] A. M. Durand, D. P. Belanger, C. H. Booth, F. Ye, S. Chi, J. A. Fernandez-Baca, and M. Bhat, *J. Phys.: Condens. Matter* **25**, 382203 (2013).
- [18] G. E. Sterbinsky, P. J. Ryan, J.-W. Kim, E. Karapetrova, J. X. Ma, J. Shi, and J. C. Woicik, *Phys. Rev. B* **85**, 020403 (2012).
- [19] Q. Wei, T. Zhang, X. P. Wang, and Q. F. Fang, *Eur. Phys. J. Appl. Phys.* **57**, 30401 (2012).
- [20] C. Hu, K. Park, A. Posadas, J. Jordan-Sweet, A. Demkov, and E. Yu, *J. Appl. Phys.* **114**, 183909 (2013).
- [21] R. Corp., The Rigaku Journal **26**, 1 (2010).
- [22] J. Rodriguez-Carvajal, FULLPROF: A program for Rietveld refinement and pattern matching analysis, Powder Diffraction, satellite meeting of the XVth IUCr congress (1990).
- [23] S. Thota, A. Kumar, and J. Kumar, *Mat. Sci. and Eng. B* **164**, 30 (2009).
- [24] N. Menyuk, K. Dwight, and P. M. Raccach, *J. Phys. Chem. Solids* **28**, 549 (1967).
- [25] J. Androulakis, N. Katsarakis, and J. Giapintzakis, *Phys. Rev. B* **64**, 174401 (2001).
- [26] M. A. Senaris-Rodriguez and J. B. Goodenough, *J. Sol. State Chem.* **118**, 323 (1995).
- [27] V. V. Sikolenko, E. V. Pomjakushina, and S. Y. Istomin, *J. Magn. and Magn. Mater.* **258**, 300 (2003).
- [28] G. Thornton, B. C. Tofield, and A. W. Hewat, *J. Sol. St. Chem.* **61**, 301 (1986).
- [29] J. Wu and C. Leighton, *Phys. Rev. B* **67**, 174408 (2003).
- [30] S. R. English, J. Wu, and C. Leighton, *Phys. Rev. B* **65**, 220407 (2002).
- [31] S. R. Giblin, I. Terry, D. Prabhakaran, A. T. Boothroyd, J. Wu, and C. Leighton, *Phys. Rev. B* **74**, 104411 (2006).
- [32] V. Golovanov, L. Mihaly, and A. R. Moodenbaugh, *Phys. Rev. B* **53**, 8207 (1996).
- [33] P. G. Radaelli and S.-W. Cheong, *Phys. Rev. B* **66**, 094408 (2002).
- [34] R. P. P. A. Korzhavyi, H. Fjellvag, and A. Kjekshus, *Phys. Rev. B* **60**, 16423 (1999).
- [35] A. Mineshige, M. Kobune, S. Fujii, Z. Ogumi, M. Inaba, T. Yao, and K. Kikuchi, *J. Sol. St. Chem.* **142**, 374 (1999).
- [36] K. Asai, O. Yokokura, N. Nishimori, H. Chou, J. M. Tranquada, G. Shirane, S. Higuchi, Y. Okamima, and K. Kohn, *Phys. Rev. B* **50**, 3025 (1994).
- [37] K. Binder and P. C. Hohenberg, *Phys. Rev. B* **6**, 3461 (1972).
- [38] K. Binder and P. C. Hohenberg, *Phys. Rev. B* **9**, 2194 (1974).
- [39] J.-Q. Yan, J.-S. Zhou, and J. B. Goodenough, *Phys. Rev. B* **70**, 014402 (2004).
- [40] D. Fuchs, L. Dieterle, E. Arac, R. Eder, P. Adelman, V. Eyert, T. Kopp, R. Schneider, D. Gerthsen, and H. v. Lohneysen, *Phys. Rev. B* **79**, 024424 (2009).
- [41] M. Itoh, M. Sugahara, I. Natori, and K. Motoya, *J. Phys. Soc. Jpn.* **64**, 3967 (1995).
- [42] K. Knizek, P. Novak, and Z. Jirak, *Phys. Rev. B* **71**, 054420 (2005).
- [43] I. Fita, D. Mogilyansky, V. Markovich, R. Puzniak, A. Wisniewski, L. Titelman, L. Vradman, H. Herskowitz, V. N. Varyukhin, and G. Gorodetsky, *Journ. of Non-Crystalline Solids* **354**, 5204 (2008).
- [44] A. Harada, T. Taniyama, Y. Takeuchi, T. Sato, T. Kyomen, and M. Itoh, *Phys. Rev. B* **75**, 184426 (2007).